

*Full Research Paper*

## **An Electronic Measurement Instrumentation of the Impedance of a Loaded Fuel Cell or Battery**

**El-Hassane Aglzim<sup>1,\*</sup>, Amar Rouane<sup>1</sup> and Reddad El-Moznine<sup>2</sup>**

1 Laboratoire d'Instrumentation Electronique de Nancy (L.I.E.N.), Nancy Université, Boulevard des Aiguillettes, BP239 - 54506 Vandoeuvre les Nancy, France. E-mail: el-hassane.aglzim@lien.uhp-nancy.fr; amar.rouane@lien.uhp-nancy.fr

2 Physical Laboratory of the Condensed Matter (L.P.M.C.), Université Chouaib Doukkali, Route Ben Maachou, BP20 - 24000 El Jadida, Morocco. E-mail: elmoznine@yahoo.fr

\* Author to whom correspondence should be addressed. El-hassane.aglzim@lien.uhp-nancy.fr

*Received: 30 August 2007 / Accepted: 16 October 2007 / Published: 17 October 2007*

---

**Abstract:** In this paper we present an inexpensive electronic measurement instrumentation developed in our laboratory, to measure and plot the impedance of a loaded fuel cell or battery. Impedance measurements were taken by using the load modulation method. This instrumentation has been developed around a VXI system stand which controls electronic cards. Software under Hpvvee<sup>®</sup> was developed for automatic measurements and the layout of the impedance of the fuel cell on load. The measurement environment, like the ambient temperature, the fuel cell temperature, the level of the hydrogen, etc..., were taken with several sensors that enable us to control the measurement. To filter the noise and the influence of the 50Hz, we have implemented a synchronous detection which filters in a very narrow way around the useful signal. The theoretical result obtained by a simulation under Pspice<sup>®</sup> of the method used consolidates the choice of this method and the possibility of obtaining correct and exploitable results. The experimental results are preliminary results on a 12V vehicle battery, having an inrush current of 330A and a capacity of 40Ah (impedance measurements on a fuel cell are in progress, and will be the subject of a forthcoming paper). The results were plotted at various nominal voltages of the battery (12.7V, 10V, 8V and 5V) and with two imposed currents (0.6A and 4A). The Nyquist diagram resulting from the experimental data enable us to show an influence of the load of the battery on its internal impedance. The similitude in the graph form and in order of magnitude of the values obtained (both theoretical and practical) enables us to validate our electronic measurement instrumentation. One of the future uses for this instrumentation is to integrate it with several

control sensors, on a vehicle as an embedded system to monitor the degradation of fuel cell membranes.

**Keywords:** fuel cell on load, impedance measurements, electrochemical impedance spectroscopy

---

## 1. Introduction

The challenges in energy and climatic conditions are now very well established. The use of hydrogen in fuel cell is an essential vector, and has been the focus of intensive study in recent years as promising alternative energy sources. Thus, various studies have been carried out in the electronic-physic domain of these kinds of generator [1] [2]. Impedance measurement is a powerful technique, which can provide useful information on the electro-chemical systems in a real and very short time [3]. This technique can be considered as a good tool to determine the state of charge of batteries or fuel cells.

To bring a solution to the optimization of the powers of the fuel cells, we invested within the Laboratory of Electronic Instrumentation of Nancy (L.I.E.N) in the development and the realization of a system for the impedance measurement of a fuel cell on load using electronic cards and sensors. Most of impedance measurements on fuel cells are made without load. Impedance measurement on a battery or fuel cell with load is very important in order to examine the influence of this latter, on its performance. For these reasons, we are interested in the development and the realization of a system in order to achieve impedance measurement of a battery or fuel cell on load, in our laboratory. This system is based on the electrochemical impedance spectroscopy (EIS) method for measuring and plotting the diagram Nyquist of battery or fuel cell impedance. The analysis and the shape of the diagram can provide information about the state of charge of the sample under test.

## 2. Theoretical Consideration

### 2.1. Method

A simulation test under Pspice<sup>®</sup> was developed in order to validate the choice of our method and its ability to provide some accurate and exploitable results. The electrical model to represent the different components is given in Figure 1. The variable load is represented by a MOSFET, and the internal impedance of the fuel cell is represented by Randle's circuit ( $R_{ohm} = 10\text{m}\Omega$ ,  $R_{act} = 90\text{m}\Omega$ , and  $C_{dc} = 300\mu\text{F}$ ). These values correspond to what one can expect for a PEM fuel cell. These estimated values are based on the work carried out by Noponen [7], Wagner [8] and Brunetto and al. [9]. The later other did measurement on PEMFC with the same dimensions as our fuel cell on which the experimental measurements are expected to be done. They found that the real part is ranging from  $3\text{m}\Omega$  and  $200\text{m}\Omega$  and the imaginary part is close to  $15\text{m}\Omega$ .

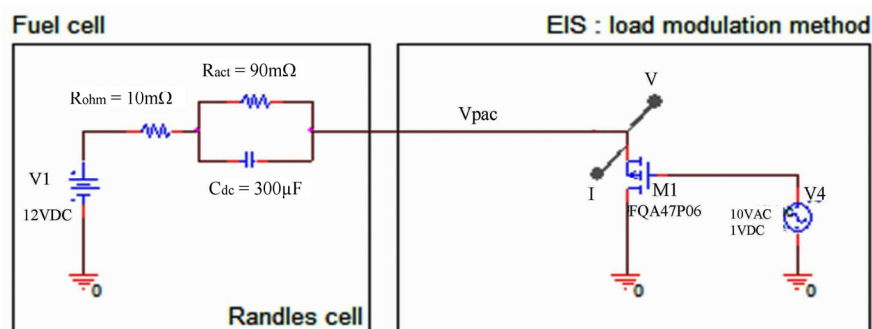


**Figure 1.** Schematic diagram of the electrical method used for simulation.

## 2.2. Results

The frequency range used in this simulation used here is the same for the experimental measurement. It is ranging from some mHz to 10 kHz. Figure 2 shows the result of this simulation in the Nyquist graph, where the imaginary part ( $Z''$ ) versus the real part ( $Z'$ ) of the complex impedance is plotted. A perfect semi-circle is obtained. Also as it can be seen, the negative sign before the imaginary part ( $Z''$ ). The results of this simulation allowed us to make a comparison with experimental results in order to validate this method and to examine its feasibility.

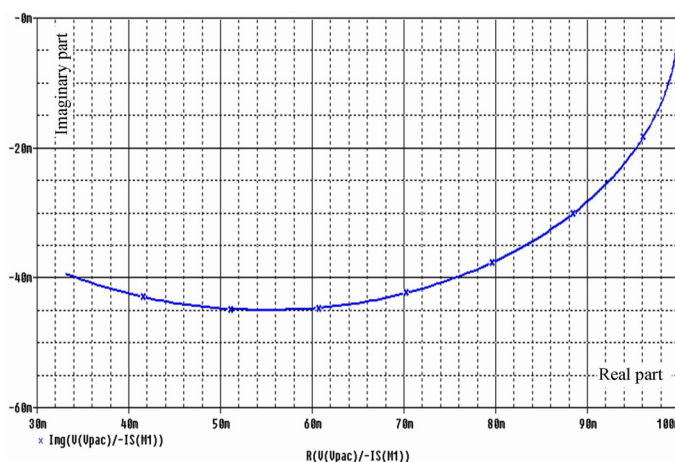


**Figure 2.** Imaginary part ( $Z''$ ) of the complex impedance ( $Z^*$ ) versus real part ( $Z'$ ), Nyquist plot simulation.

## 3. Experimental Study

### 3.1. Method

The Electrochemical Impedance Spectroscopy (EIS) has the advantage, compared to other methods, to have a less influence on battery or fuel cell during the working of these latter. It can provide more information on the state of the charge. Measurements are generally carried out without load. It is useful to cover a large frequency range in order to obtain more information from the impedance spectrum generated. For a PEM fuel cell, the impedance spectrum was generated in a frequency ranging from 1Hz to 10 kHz [4]. However, Walkiewicz and al [5] did studies between 1mHz and 65KHz. The number of points collected by decade varies between 8 and 10 points. The principle of

measurement is to add a signal, at constant frequency, to the output of the voltage of the battery when this latter is delivering the desired current. The superimposed signal can be obtained by three methods: potentiostatic, galvanostatic or load modulation methods.

Among of these three later methods, we have selected the load modulation method. It consists in varying the resistance of the load according to the signal that we would like to superimpose. Thus, the impedance of battery or fuel cell under test can be obtained by the ratio of the voltage of the battery and the current coming from the battery. Figure 3 shows an electric representation of this method.

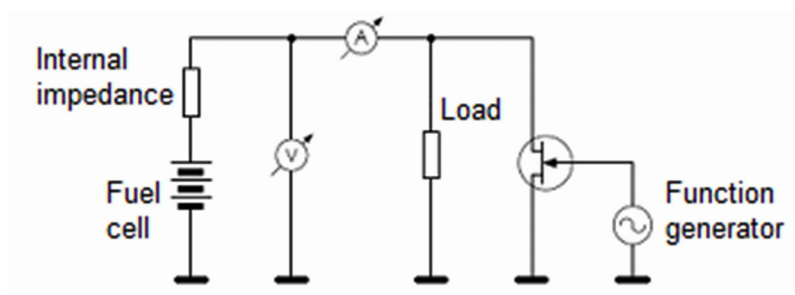


**Figure 3.** Principle of the load modulation method [6].

### 3.2. Principle of the test bench

The principle of the measurement using the test bench developed in our laboratory is presented in Figure 4. The current is controlled by an analogical current regulation. This allows us to have a more linear, fast and reliable regulation.

The instrumentation is developed around a VXI system stand, which controls different electronic cards. Software, under Hpvée<sup>®</sup>, was developed for automatic impedance measurements of the device under test (DUT). In order to filter the noise and to avoid the influence of the 50Hz, a synchronous detection was used, which filters a very narrow way around the useful signal. Thus, it is possible to filter all the noise and to detect the amplitude of the useful signal at frequency fixed. Two synchronous detections were used: the first is used for the imposed current to the device under test, while the second is used for the response of the voltage of this same device. These two synchronous detections are controlled by four square signals delivered by an electronic card, which are out phase of 90°. The output of this synchronous detection allowed us to collect the real and imaginary part of the current and voltage, as well as, their respective phases. The real and imaginary part of the impedance of the DUT is calculated then by using the ohm's law. These two parameters (real and imaginary part of the complex impedance) can be plotted in the Nyquist diagram.

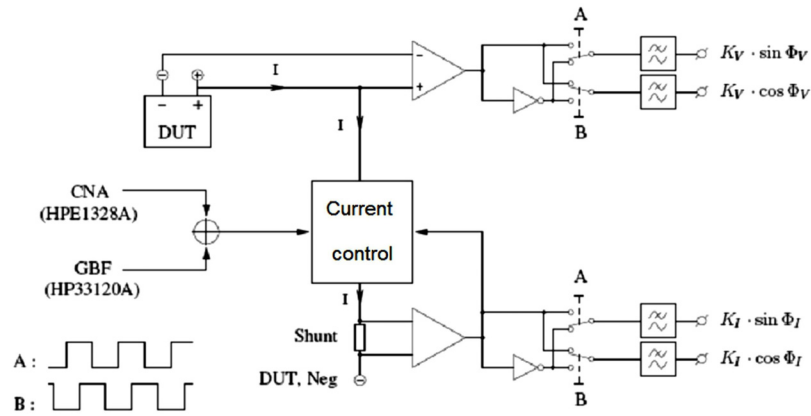


Figure 4. Synoptic of the test bench.

The system developed, by our own, can support an active current up to 50A on the load. The new achievement in this work results in the possibility to better understand and to study the fuel cell in its environment when it is delivering current on load such as electric motor. In this case, the measurement and the analysis of the impedance are a good tool, which can give useful information about the state of the battery. For a better comprehension of the system operation, we make a more detailed description below.

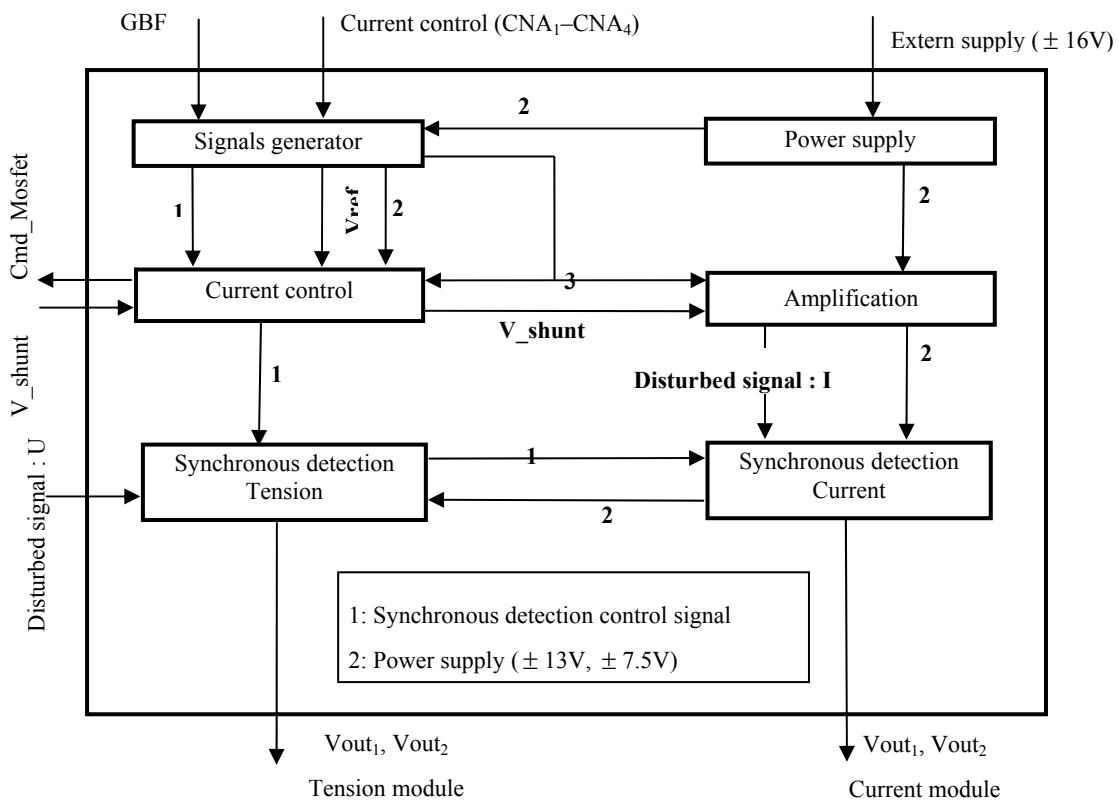
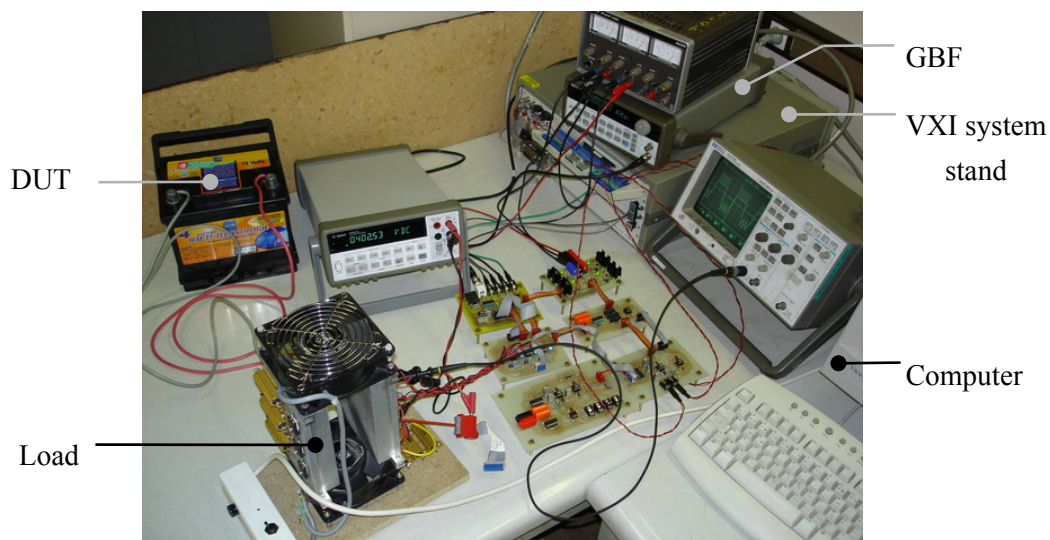


Figure 5. Systemic representation of the test bench.

The instrumentation is controlled by an Hpvee® program developed for this project. This program controls a VXI system stand containing several measuring devices in the form of plug-in circuits: a GBF (HPE1340A), a multimeter (HPE1326B), a 4-Channel D/A Converter (HPE1328A), a multiplexer 16 ways (HPE1351A) and an input/output circuit (HPE1330B). The “Power supply”

module provides the supply to the various electronic circuits, it delivers a tension of  $\pm 13\text{V}$  and  $\pm 7.5\text{V}$ . The “Signals generator” module provides the control square signals for the synchronous detections of the tension and the current, as well as the current imposed signal. These signals are generated from the sinusoidal signal delivered by the GBF. The frequencies scanning is controlled by the Hpvce<sup>®</sup> program, which changes the frequency value step by step defines after the measurement of  $V_{out_1}$  and  $V_{out_2}$  of the tension and the current. The “Current control” module drives the load by an imposed current while running. This current is a square signal, generated by the “Signals generator” module; it is composed of a DC part which represent the imposed current and an AC part which represents the frequency on which this current is imposed. The “Amplification” module amplifies the imposed current signal, measured at the Shunt resistance terminals. This amplified signal which is disturbed is transmitted to the synchronous detection (current). The “Synchronous detection” module allows the amplification of the signal coming from the DUT, and the recovery of the real and imaginary part of this signal by the synchronous detection.



**Figure 6.** Test bed for the impedance measurement of a fuel cell on load.

### 3.2.1. “Power Supply” module

The “Power supply” module in figure 7, manages the generation and the distribution of the various tensions which are necessary to supply the active elements of all the other modules. It transforms the tensions of  $\pm 16\text{ V}$  to a  $\pm 13\text{ V}$  and  $\pm 7.5\text{ V}$  tensions. Two diodes at the input allow the protection of the module in the event of a surge or a bad polarization.

We decided to create this module to allow the circuit to be autonomous and to be embedded in a vehicle. Its finality being to be an embedded system, we were to avoid being dependent on any external power supply. The external supply which provides the  $\pm 16\text{ V}$  can be replaced by batteries. For our tests and for the measurements, we used a simple laboratory power supply. In the future, this supply must be provided by the fuel cell.

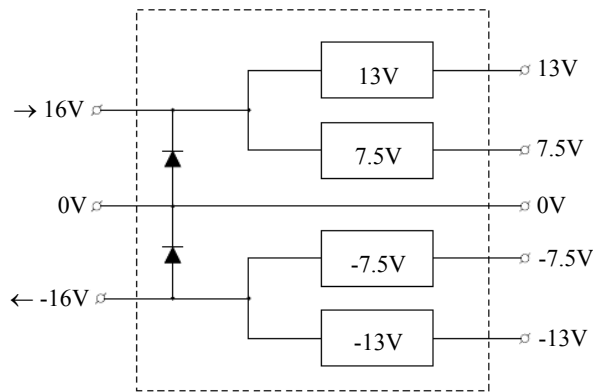


**Figure 7.** Schematic of the “Power supply” module.

### 3.2.2. “Signals generator” module

The “Signals generator” module is useful like interfaces for all the input signals. It converts the square signal coming from the GBF and the tensions provided by the D/A Converter which adjusts the current and which chooses the amplification of the signal. This module amplifies and filters all the input signals. Starting from the signal provides by the GBF, it generates four square signals of the same frequency, out of phase of  $0$ ,  $\pi/2$ ,  $\pi$  and  $3\pi/2$ . These signals allow the commutation of the quad bilateral switch (CD4066) on the synchronous detection module. The fuel cell output current will be controlled by the  $CNA_1$  tension superimposed with one of the four outputs of the phase-converter. For that, the “Signals generator” module carries out the addition between these two signals.

The  $CNA_2$  to  $CNA_4$  tensions are used for the choice of the measuring range. The signal AC is not provided any more by the GBF, but by the output of the CMOS quad bilateral switches. Behind the phase-converter and before the adder, tension dividers (which we can select with three relays) determine three levels of amplification, allowing a measurement over three decades of impedance.

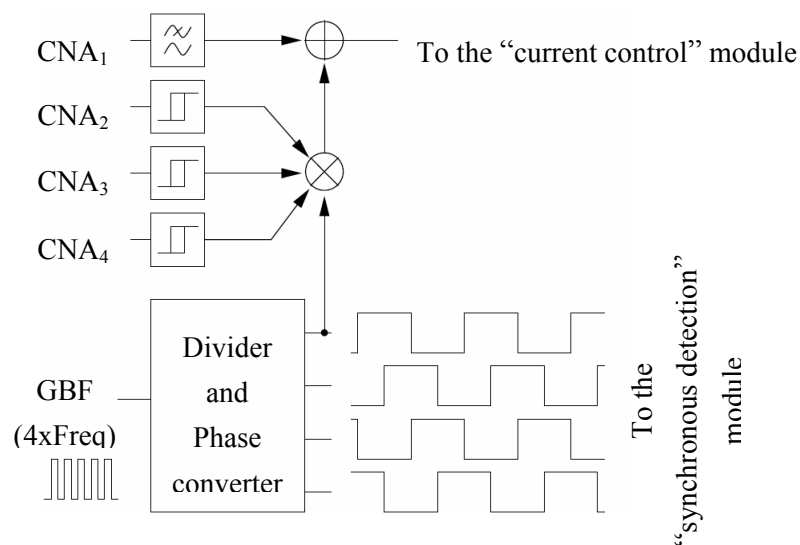
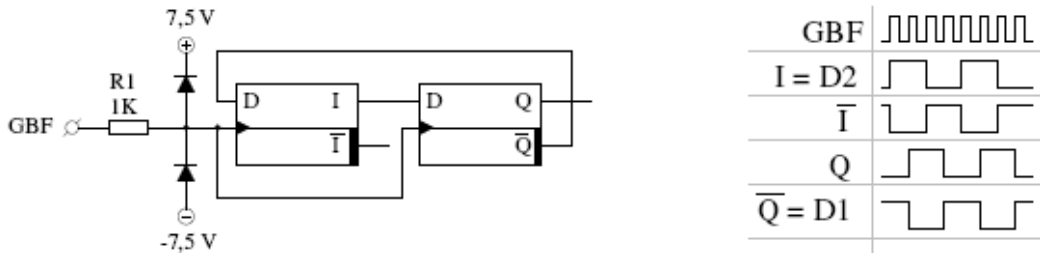


**Figure 8.** Schematic of the “Signals generator” module.



a) The phase-converter

b) Output signals driving the synchronous detection module

**Figure 9.** The phase converter and its outputs signals.

3.2.3. “Current control” module

This module regulates the current output by the fuel cell. It is a circuit which appears on page 382 of the book “The Art of Electronics” [10]. The operational amplifier regulates the current going from DUT,POS to DUT,NEG via the MOSFET according to the  $V_{ref}$  tension. The adjustments and the choice of the components are made to have for a  $V_{ref}$  tension of 1V, an equivalent current of 1A. The tension measured on the shunt resistance terminals, is the image of the imposed current. 100mV of this tension corresponds to a current of 1A. The tension measured at the terminals of the DUT corresponds to the response in tension of the DUT to the imposed current. These two tensions will enable us to define the impedance of the DUT by using the Ohm’s law, and that by making the extraction of the real and imaginary part of the current and the tension.

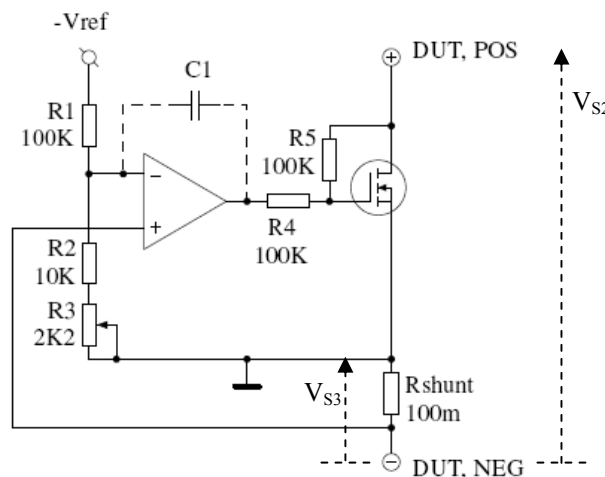


**Figure 10.** Schematic of the “Current control” module.

We can observe below in figure 11, the results obtained by the current control module. Figure 11.a and figure 13.b show the signal ( $V_{S3}$ ) obtained at the shunt resistance terminals. We have a square signal which corresponds to the current image with an amplitude of 400mV corresponding to a 4A current. Figure 11.b and figure 13.b show the signal ( $V_{S2}$ ) obtained at the DUT terminals which corresponds to the response in tension of the imposed current. It has an amplitude of 200mV. With these two

parameters, we can determine the real part of the impedance by dividing the tension by the current. In this case and with this measurement values, the real part is of 50mΩ.

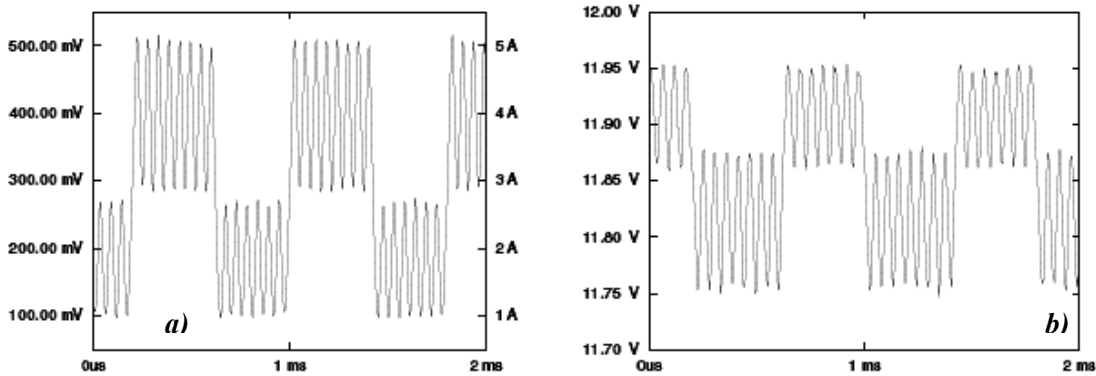


**Figure 11.** a) Image of the current imposed to the DUT (100mV = 1A) |  $V_{S3}$  of figure 13.b  
 b) Response in tension coming from the DUT |  $V_{S2}$  of figure 13.b.

3.2.4. “Amplification” module

This module amplifies the alternate component of the tension around the resistance of shunt before providing the signal amplified to synchronous detection. The principal constraint of this module is a weak offset of tension because this last is not filtered by synchronous detection. Moreover, amplification must be eligible in order to use all the dynamics of synchronous detection to reach a better resolution and to decrease the errors introduced by the offsets of tension. The circuit must also have an output with the reversed signal and a second with the not-reversed signal. These two signals are used for synchronous detection. The circuit is presented below in figure 12.

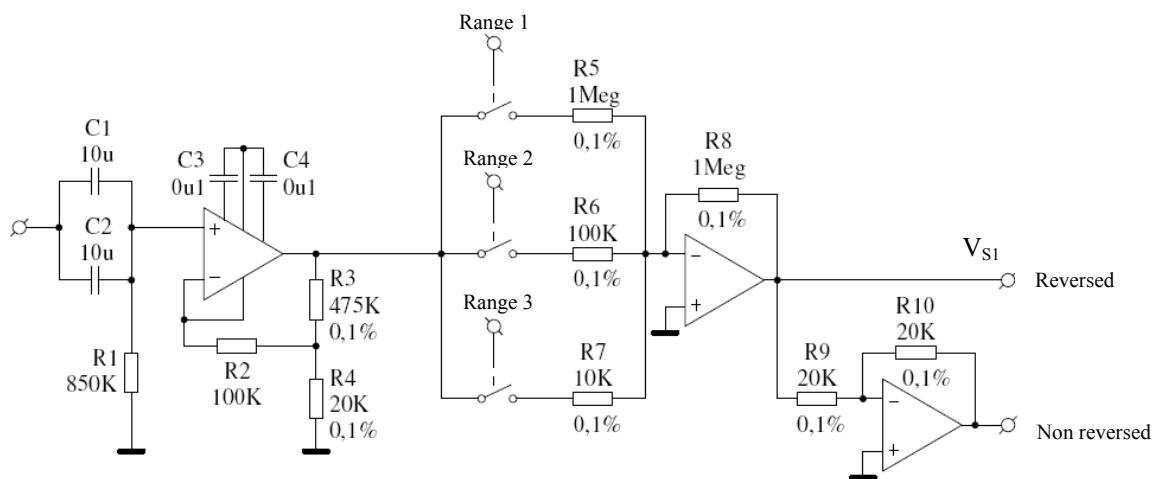


**Figure 12.** Schematic of the “Amplification” module.

Figure 13 shows the results of measurement carried out on this module. For measurement presented on figure 13.a, the input was excited by a sinusoidal signal with an amplitude of 50mV, provided by

the GBF. The amplification rate is a function of the used relay: 23 for relay 1 (range 1), 230 for relay 2 (range 2) and 2300 for relay 3 (range 3). If the third relay is open, amplification is so high that the exit becomes saturated. For measurement presented in figure 13.b, an amplification of the signal at the shunt resistance terminals is made. Its continuous component is filtered by the input capacitive of the module before an amplification by 23. It is noticed that the square signal is rounded a little compared to former measurement. This is due to the reduced band-width of the amplification module due to the Unity Gain Bandwidth of the AOP ICL7650SCPD.

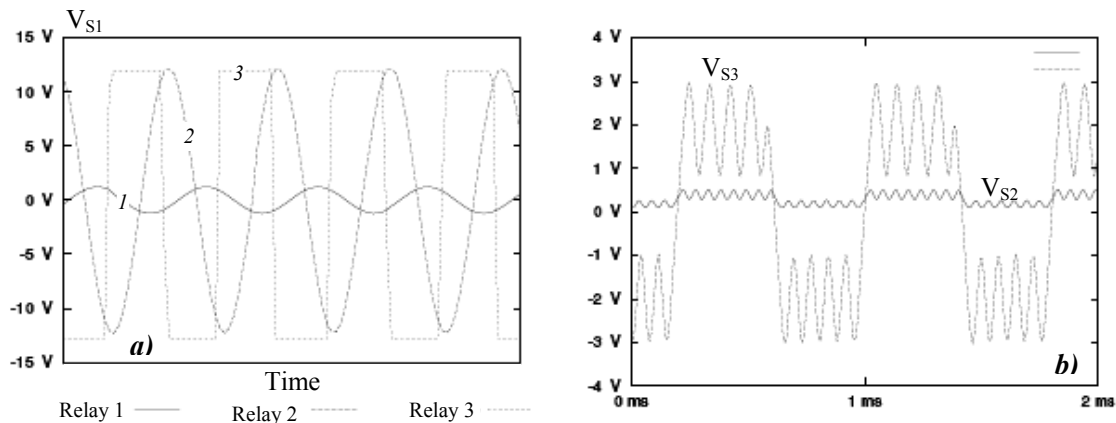


**Figure 13.** a) Amplification according to the position of the relay  
b) Amplification of the tension measured at the shunt resistance terminals

### 3.2.5. “Synchronous detection” module

The synchronous detection of our test bed is composed of two basic elements. These two elements obtain the same input signal, but two different signals of reference out of phase from exactly  $90^\circ$ . In this case, when the first phase detector has an output signal of:

$$V_{out_1} = \frac{2E}{\pi} \cos(\phi) \quad (1)$$

the second detector presents a signal of :

$$V_{out_2} = \frac{2E}{\pi} \sin(\phi) \quad (2)$$

at its output. Considering that:

$$\sin^2(\Phi) + \cos^2(\Phi) = 1 \quad (3)$$

we can calculate :

$$V^2_{out_1} + V^2_{out_2} = \left(\frac{2E}{\pi}\right)^2 (\sin^2(\phi) + \cos^2(\phi)) \quad (4)$$

We can deduce that:

$$E = \frac{\pi}{2} \sqrt{V^2 out_1 + V^2 out_2} \quad (5)$$

By using another law of trigonometry, we can obtain the phase of the signal:

$$\phi = \arctan\left(\frac{Vout_2}{Vout_1}\right) \quad (6)$$

To calculate the real and the imaginary part of the signal, it is enough to know that:

$$\text{Re}(E) = E \cos(\phi) \quad (7)$$

$$\text{Im}(E) = E \sin(\phi) \quad (8)$$

Since a synchronous detection can measure only one magnitude at the same time (either the current, or the tension), we put two of them for the measurement of the current and the tension simultaneously to determine the impedance of the DUT on load.

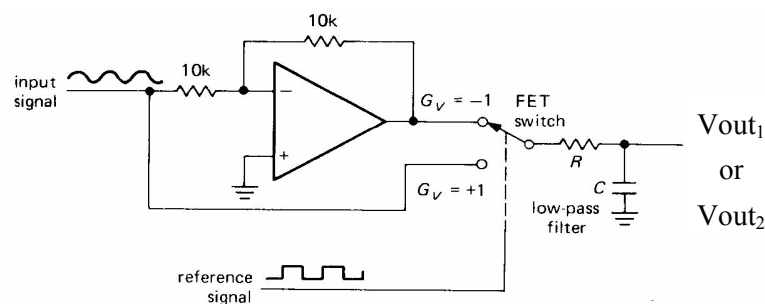


**Figure 14.** Principle of the synchronous detection module [10].

#### 4. Results and Discussion

The preliminary results have been carried out on a vehicle battery delivering a starting current of 330A and having a capacity of 40Ah (impedance measurements on a PEM fuel cell on load are in progress). The impedance Nyquist graph of a fuel cell and a vehicle battery are very close [11] [12] because the electrochemical processes are almost identical [13]. This gives us the possibility to make measurement test on a vehicle battery. However, spectrums are very depending to the values of components used in the modelization of the Randles circuit.

Measurements were carried out at different nominal voltages (12.7V, 10V, 8V and 5V) with two imposed currents (0.6 A and 4A). The choice of these limits current is arbitrary. Figure 15 and 16 show the complex plane impedance plots (Nyquist diagram). The results obtained enable us to show the influence of the load on its impedance. Nyquist Graphs showed below were obtained by using the

software Hpvce<sup>®</sup> developed for the opportunity it is then transposed under Microsoft<sup>®</sup> Excel in order to plot the curves. Nyquist graphs are generally presented in the literature have a positive imaginary axis. Actually, values on the axis of the imaginary part are negative (effect capacitor), but by convention, at the time of the tracing of the graph, they are multiplied by -1. In order to visualize the different phenomena and the effects occurring inside the battery, basically capacitor effect, we prefer to keep the negative imaginary axis.

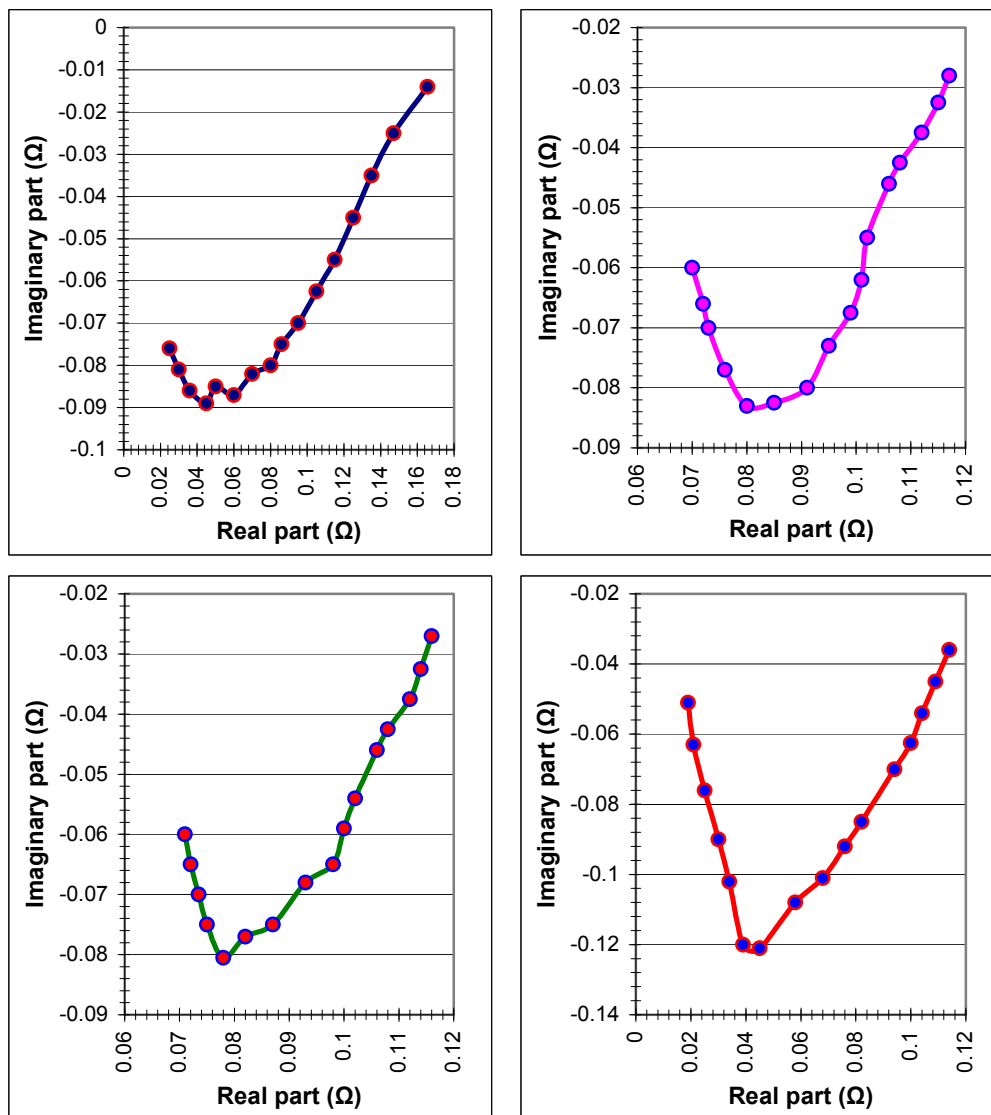


**Figure 15.** Impedance of the battery at an imposed current of 0.6A and at nominal voltage of:  
 a) 12.7V    b) 10V    c) 8V    d) 5V.

As it can be seen, the shape of the curves shown in Figure 15 demonstrates the ability of our system to measure the impedance of a DUT on load. The shape of the curve obtained at a nominal voltage of 12.7V and at current imposed of 0,6A is similar to the shape of the theoretical curve shown in figure 2 using the simulation. As it can be seen, the curve become more linear when the nominal voltage of the battery decreases, which means a discharge of this latter. This phenomenon can be seen for a nominal voltage of 5V (Figure 15.d). A pseudo semi-circle obtained if we do not take into account of the right

stiffness. The shape of this curve could be due to the weak nominal voltage at which this measure has been made. Below a nominal voltage of 4V, our system of measure is not more capable to make some correct and exploitable measurement. This could be due to the level of tension drain/source of the Mosfets that must be important enough for measurement. The experimental curves show the predicted behavior by the theory at low frequencies. Resistive effect is generated by a positive value at the level of the real axis, while capacitor effect by negative value at the level of the imaginary axis. We can also observe a variation of component values, basically resistances of diffusion, with the discharge of the battery. The second set of measurement at imposed current of 4A (Figure 16) show that the curves have the same shape to those obtained with at imposed current of 0.6A (Figure 15), however, values of real and imaginary axes are different.

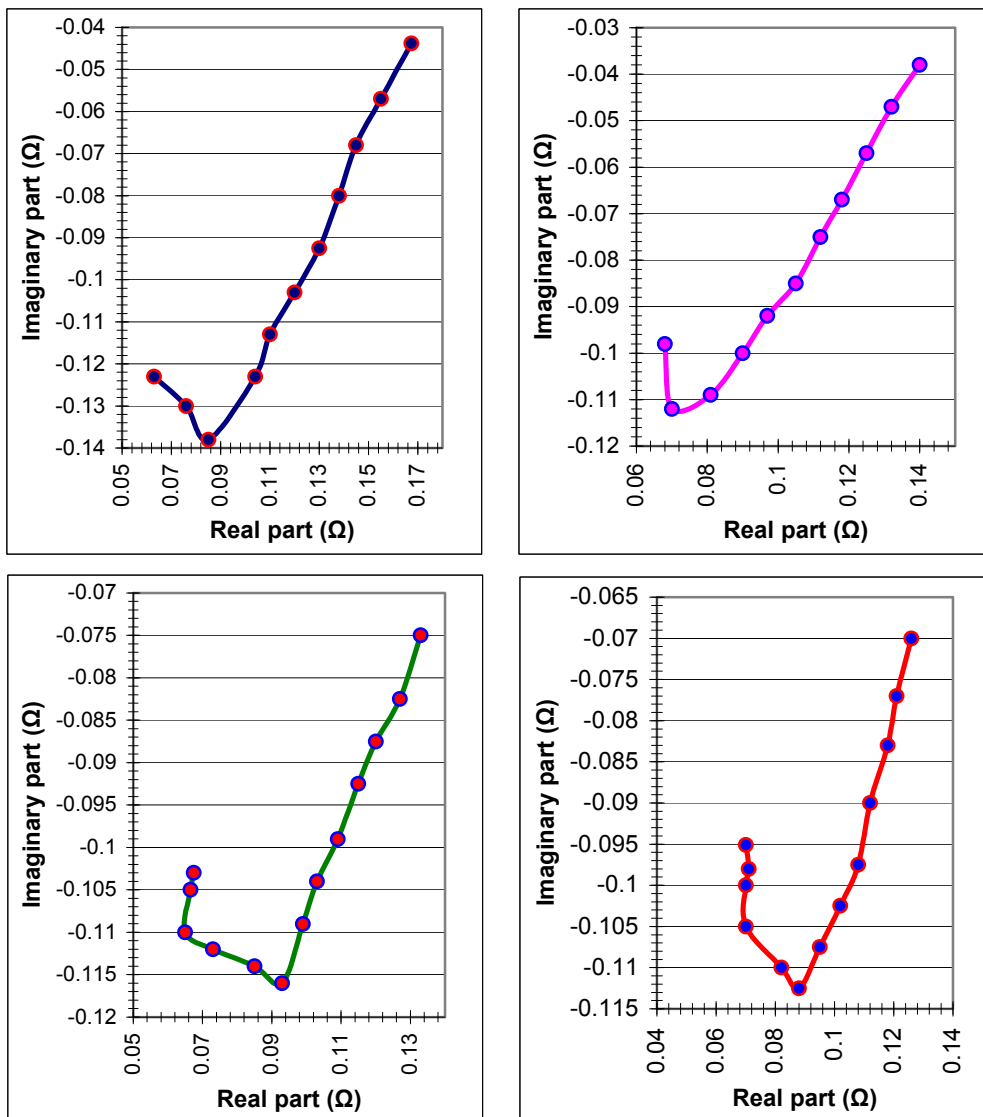


**Figure 16.** Impedance of the battery at an imposed current of 4A and at nominal voltage of:  
 a) 12.7V    b) 10V    c) 8V    d) 5V.

## 5. Conclusion

The impedance measurement is a very powerful tool for controlling the state of battery. The theoretical model of the method used has been simulated under Pspice<sup>®</sup>. This study was necessary to validate our concept by comparing theoretical and experimental results.

In the theoretical part, we gave the principle of measurement and the description of our test bench, as well as, the different electronic cards. Results of simulation reinforce us in the idea that the way that has been followed for the development of this band measurement was good. The experimental part shows also the ability of the developed system to measure the impedance of a vehicle battery, and therefore it could be used also to measure the impedance of the fuel cell at various nominal voltages.

The first aim of these tests is to validate our method and to compare the experimental results with those obtained using the simulation under Pspice<sup>®</sup>. On the other hand these testes can also confirm the choice of the method of load modulation, and the good electronic card working developed for this end. The different Nyquist graphs show that a relationship could exist therefore between the state of load and the internal impedance of the DUT. In the case of the lead battery, as the one used in this study, the variation of the impedance is generally weak (in the order of milliohms) in the frequency range used. The correlation between the theoretical and experimental curves can confirm that our test bench allows to measure and to plot the impedance of a battery or fuel cell in frequencies. In the future we are interesting by adding humidity sensors to be able to compare and to correlate the impedance of the fuel cell on load with the humidity level inside it. This correlation will give us informations on the membrane degradation. This equipment could be integrated in a vehicle functioning with a fuel cell in order to control the deterioration of its membranes by using data from control sensors and measurement equipments.

## Acknowledgments

The authors would like to thank the Lorraine region – France – for supporting this work.

## References and Notes

1. Easton, E.B.; Pickup, P.G. An electrochemical impedance spectroscopy study of fuel cell electrodes. *Electrochimica Acta* **2005**, *50*, 2469–2474.
2. Jasinski, P.; Suzuki, T.; Dogan F.; Anderson, H.U. Impedance spectroscopy of single chamber SOFC. *Solid State Ionics* **2004**, *175*, 35–38.
3. Li, G.; Pickup, P.G. Measurement of single electrode potentials and impedances in hydrogen and direct methanol PEM fuel cells. *Electrochimica Acta* **2004**, *49*, 4119–4126.
4. *Making Fuel Cell AC Impedance Measurements Utilizing Agilent N3300A Series Electronic Loads*; Product Note for Agilent Technologies, Inc.: Santa Clara, CA, 2002.
5. Walkiewicz, S. *Étude par spectroscopie d'impédance électrochimique de piles à combustibles à membrane échangeuse de protons* (in French); DEA Électrochimie, Institut National Polytechnique de Grenoble ENSEEG, Grenoble, France, 2001.
6. Kraemer, B. *Mesure par spectroscopie de l'impédance d'une pile à combustible en charge* (in French); DEA Report, UHP Nancy1, Nancy, France, 2005.

7. Noponen, M. Current Distribution measurements and Modelling of Mass Transfer in Polymer Electrolyte Fuel Cells. Ph.D. Thesis, Helsinki University of Technology, March 2004.
8. Wagner, N. Characterization of membrane electrode assemblies in polymer electrolyte fuel cells using AC impedance spectroscopy. *Journal of Applied Electrochemistry* **2002**, *32*, 589–863.
9. Brunetto, C.; Tina, G.; Squadrito, G.; Moschetto, A. PEMFC Diagnostics and Modelling by Electrochemical Impedance Spectroscopy. *IEEE MELECON* **2004**, *3*, 1045–1050.
10. Horowitz, P.; Hill, W. *The Art of Electronics*, 2<sup>nd</sup> Ed.; Cambridge University Press: Cambridge, 1989.
11. Diard, J.P.; Le Gorrec, B.; Montella, C.; Poinsignon, C.; Vitter, G. Impedance Measurements of Polymer Electrolyte Membrane Fuel Cells Running on Constant Load. *Journal of Power Sources* **1998**, *74*, 244–245.
12. Diard, J.P.; Le Gorrec, B.; Montella, C. EIS Study of Electrochemical Battery discharge on constant load. *Journal of Power Sources* **1998**, *70*, 78–84.
13. Jörn, A.T. Multiple Model Impedance Spectroscopy Techniques for testing Electrochemical Systems. *Journal of Power Sources* **2004**, *136*, 246–249.